Future Detection of Supernova Neutrino Burst and Explosion Mechanism

T. Totani
Department of Physics, The University of Tokyo, Tokyo 113 Japan
E-mail: totani@utaphp2.phys.s.u-tokyo.ac.jp

K. Sato
Research Center for the Early Universe, The University of Tokyo, Tokyo 113 Japan

and

H.E. Dalhed and J.R. Wilson
Lawrence Livermore National Laboratory
7000 East Avenue, L-015, Livermore, CA94550, U.S.A.

ABSTRACT

Future detection of a supernova neutrino burst by large underground detectors would give important information for the explosion mechanism of collapse-driven supernovae. We studied the statistical analysis for the future detection of a nearby supernova by using a numerical supernova model and realistic Monte-Carlo simulations of detection by the Super-Kamiokande detector. We mainly discuss the detectability of the signatures of the delayed explosion mechanism in the time evolution of the $\bar{\nu}_e$ luminosity and spectrum. For a supernova at 10 kpc away from the Earth, we find that not only the signature is clearly discernible, but also the deviation of energy spectrum from the Fermi-Dirac (FD) distribution can be observed. The deviation from the FD distribution would, if observed, provide a test for the standard picture of neutrino emission from collapse-driven supernovae. For the $D = 50$ kpc case, the signature of the delayed explosion is still observable, but statistical fluctuation is too large to detect the deviation from the FD distribution. We also propose a method for statistical reconstruction of the time evolution of $\bar{\nu}_e$ luminosity and spectrum from data, by which we can get a smoother time evolution and smaller statistical errors than a simple, time-binning analysis. This method is useful especially when the available number of events is relatively small, e.g., a supernova in the LMC or SMC. Neutronization burst of ν_e's produces about 5 scattering events when $D = 10$ kpc and this signal is difficult to distinguish from $\bar{\nu}_e p$ events.

1. Introduction

Although the Type II (and Ib, Ic) supernovae are generally believed to be associated with gravitational collapses of massive star cores at the end of their life, the explosion mechanism of the collapse-driven supernova has not yet been clarified. Two possible scenarios are so far discussed: the prompt (Wilson 1971; Hillebrandt 1982; Arnett 1983; Hillebrandt, Nomoto, & Wolff 1984; Baron, Cooperstein, & Kahana 1985) or delayed (Wilson 1985; Bethe & Wilson 1985) explosion. If the prompt explosion obtains, the envelope of progenitor stars is directly expelled on the time scale of ~ 10 msec by the shock wave, which is generated by the core bounce when collapse has compressed the inner core of massive stars up to supranuclear densities. It is known that, however, this mechanism can work only when the progenitor star is relatively small ($\sim 10 M_{\odot}$) and equation of state is soft enough, otherwise the shock wave loses its energy by photodissociation of heavy nuclei and neutrino emission behind the shock front, and finally stalls. Therefore the delayed explosion scenario, in which the stalled shock is revived by the heating of neutrinos from the nascent neutron star on the time scale of ~ 1 sec, is considered to be likely.

Since electromagnetic waves cannot convey to us any information of dense and deep region relevant to the explosion mechanism, the detection of a neutrino burst by large underground detectors is almost the only chance to get some observational clues for the explosion mechanism. Supernova neutrinos have already been detected from the supernova SN1987A, which appeared in the Large Magellanic Cloud (LMC), by the two water Čerenkov detectors, Kamiokande II (Hirata et al. 1987, 1988) and IMB (Bionta et al 1987; Bratton et al. 1988). Although these detections were epoch-making events, the small numbers of captured neutrinos (11 for Kamiokande and 8 for IMB) were unfortunately too small to tell us something about the explosion mechanism. However, an international network of second-generation neutrino detectors is now emerging on the Earth, and a future event in our Galaxy or Magellanice Clouds would give us much more detailed data necessary to understand the explosion mechanism (see, e.g., Burrows, Klein, & Gandhi 1992). Among such underground detectors, the Super-Kamiokande (SK) detector, which is about 15 times larger than the Kamiokande, has started its observation and would detect 5000–10000 $\bar{\nu}_e$'s if a supernova appeared in the Galactic Center (10 kpc away from the Earth) (Totsuka 1992; Nakamura et al. 1994). Because the signatures of the explosion mechanism are seen in the time evolution of the neutrino luminosity and spectrum, statistical reconstruction of the time evolution, that requires a large number of events, is crucially important. From this viewpoint, the SK, to which we confine ourselves in this paper, is the most suitable detector to probe the explosion mechanism because of its largest detector mass and good energy resolution, among the existing or planned detectors.

In this paper, we investigate the signatures of the delayed explosion mechanism which are observable in the time evolution of the $\bar{\nu}_e$ luminosity and spectrum at the SK, by using a numerical model of supernova neutrino emission and realistic Monte-Carlo simulations of the detection by the SK. The simplest analysis is to set many bins in the time coordinate and estimate the luminosity and average energy in each bin. However, this analysis is not sufficient to reproduce a smooth evolutionary curve and some information of detection time is also lost. We propose an analysis method based on the maximum likelihood method and cubic-interpolation, which gives natural and smooth evolution without loss of time information, and test this method by using MC data generated from the numerical supernova model.

Because the supernova neutrinos are emitted thermally, the Fermi-Dirac (FD) distribution was generally assumed in previous analyses for the SN1987A data (Loredo & Lamb 1989, and references therein). However, it is known that because the neutrino opacity changes with neutrino energy, the spectrum of neutrinos deviates from the pure FD distribution with zero chemical potential. The emergent neutrino spectrum can be considered to be a blackbody radiation from a surface whose radius varies with neutrino energy, and deficit in both the low and high energy range compared to the pure FD distribution is seen (Bruenn 1987; Mayle, Wilson, & Schramm 1987; Janka & Hillebrandt 1989; Giovanoni, Ellison, & Bruenn 1989; Myra & Burrows 1990). The rich statistics of the SK may allow us to discern this deviation, and if observed, it would provide a verification for the current theoretical picture of supernova explosion and neutrino emission. Hence we also investigate whether we can see this deviation of neutrino spectrum from the FD distribution in future observations.

In §2, we describe the numerical model of a supernova explosion used in this paper, and the features of the delayed explosion are discussed. The properties of the SK detector are summarized in §3, and Monte-Calro data generation from the numerical supernova model is also described. Statistical analysis for the MC data and its results are presented in §4, and after some discussions in §5, we summarize our results in §6.

2. Numerical Model of Supernova Explosion

We use a result of neutrino emission based on a numerical simulation of supernova explosion. The simulation is performed with the numerical codes developed by Wilson and Mayle (Mayle 1985; Wilson et al 1986; Mayle, Wilson, & Schramm 1987). The simulation is a model of the SN1987A, whose progenitor is a main-sequence star of about 20 $M_\odot$. The stellar configuration from which the explosion calculation started was supplied by Woosley

and Weaver (1991). This one dimensional simulation is performed from the onset of the collapse to 18 seconds after the core bounce in a consistent way, and the total energy emitted by this time is 2.9 $\times 10^{53}$ erg. The emitted energy in $\bar{\nu}_e$'s is 4.7 $\times 10^{52}$ erg and the average energy of $\bar{\nu}_e$'s is 15.3 MeV. Figure 1 shows the time evolution of luminosity and average energy of this model, for $\nu_e, \bar{\nu}_e$, and ν_x. [The neutrino luminosity and spectrum of supernova $\nu_\mu, \bar{\nu}_\mu, \nu_\tau$, and $\bar{\nu}_\tau$ (referred to ν_x, hereafter) are almost the same.] Figure 2 shows the snapshots of the spectral evolution of supernova $\bar{\nu}_e$'s in the form of differential number luminosity. FD spectra which have the same luminosity and average energy with zero chemical potential are also shown by dashed lines in the figure, and the deficit of both low- and high-energy neutrinos can be seen. In the following analysis, FD distributions will be introduced to provide a simple method of analyzing the possible observational data and do not represent any expected spectral shape. For generic features of supernova neutrino emission, see, e.g., Burrows et al. (1992).

Figure 3 shows the radius of selected mass points as a function of time for the present model. This model explodes by the delayed explosion mechanism, and its features are stamped onto the early evolution of neutrino luminosity and spectrum as shown in Fig. 4, in which the evolution of neutrino luminosity and average energy in the first ~ 1 second after the core bounce are shown. A characteristic of the delayed mechanism is a "hump" in the neutrino luminosity curve due to the accretion of matter onto the nascent neutron star. [This "hump" is the same with the phenomenon previously discussed in Burrows et al. (1992) as "abrupt drop in luminosity curve".] The average energy of neutrinos stays low during the hump because of the dense matter above the neutrino sphere which contributes to the neutrino opacity. The average energy gradually increases during this phase, corresponding to gradual decay of mass accretion before the delayed explosion commences. Therefore this gradual hardening of neutrino spectrum also gives another observable signature of the delayed explosion. After the accretion decays, the evolution time scale in both the luminosity and average energy becomes much longer than that in the earlier phase. The time duration of the hump in the delayed explosion is very hard to calculate from first principles so the measurement of this duration is most important for the understanding of the explosion process. On the other hand, if the prompt mechanism were viable, the envelope would be expelled in $O(10)$ msec after the core bounce and there would be no hump in the luminosity curve because of no matter accretion. The neutrino spectrum would become harder just after the core bounce and explosion, in contrast to the delayed explosion. This mechanism is likely at work for relatively low mass stars.

In the present model of supernova explosion, this hump is clearly discernible corresponding to the matter accretion during the first 0.5 [sec]. We concentrate on these two features, i.e., the hump in neutrino luminosity and increase in average energy during

the first ~ 0.5 [sec] as the signatures of the delayed explosion. It should be noted, however, that these features of the delayed explosion generally depend on the mass of initial iron cores or progenitor stars. The more massive iron cores lead to the more complicated structure in time evolution of neutrino luminosity and spectrum. In some calculations of the delayed explosion (Mayle 1985; Mayle, Wilson, & Schramm 1987), oscillatory behavior was observed whose existence may depend on the initial structure of the star.

3. Monte-Carlo Simulation of the SK detection

The Super-Kamiokande detector (Totsuka 1992; Nakamura et al. 1994) is a water Čerenkov detector whose fiducial volume for a supernova neutrino burst is 32,000 ton. We have performed Monte-Carlo (MC) simulations for the detection of supernova neutrinos by this detector, which give a data set of detection time and energy of events. We use only the time and energy information of electrons or positrons, and do not consider the directional information because positrons are emitted almost isotropically in the dominant $\bar{\nu}_e p$ reaction. The following reactions are taken into account:

$$\bar{\nu}_e + p \rightarrow e^+ + n \quad (\varepsilon_\nu^{th} = 1.8\mathrm{MeV}) \quad (\mathrm{C.C.}), \tag{1}$$

$$\nu_e\ (\bar{\nu}_e) + e^- \rightarrow \nu_e\ (\bar{\nu}_e) + e^- \quad (\mathrm{C.C.} + \mathrm{N.C.}), \tag{2}$$

$$\nu_x + e^- \rightarrow \nu_x + e^- \quad (\mathrm{N.C.}), \tag{3}$$

$$\nu_e + {}^{16}\mathrm{O} \rightarrow e^- + {}^{16}\mathrm{F} \quad (\varepsilon_\nu^{th} = 15.4\mathrm{MeV}) \quad (\mathrm{C.C.}), \tag{4}$$

$$\bar{\nu}_e + {}^{16}\mathrm{O} \rightarrow e^+ + {}^{16}\mathrm{N} \quad (\varepsilon_\nu^{th} = 11.4\mathrm{MeV}) \quad (\mathrm{C.C.}), \tag{5}$$

where C.C. and N.C. referred to charged and neutral current, respectively, and ε_ν^{th} is the threshold energy of neutrinos. For the cross sections of $\bar{\nu}_e p$ and $\nu_e(\bar{\nu}_e)^{16}\mathrm{O}$ reactions, we referred to Vogel (1984) and Haxton (1987), respectively. Although the cross sections of oxygen reactions are less certain than others, this uncertainty hardly affects the following results because of the much smaller number of events than that of the $\bar{\nu}_e p$ reaction. Recently Langanke, Vogel, & Kolbe (1996) pointed out that $(\nu, \nu' p\gamma)$ and $(\nu, \nu' n\gamma)$ reactions on $^{16}\mathrm{O}$ constitute significant signals in the observed γ-ray energy range of $\lesssim$ 10 MeV, which are not included in our MC code. The signal would allow a unique identification of ν_x, but simultaneously be a serious noise against $\bar{\nu}_e p$ events, in which we are interested here, because the SK cannot distinguish γ-rays and positrons in this energy range. In order to avoid this noise, we set the threshold energy of positron energy, $\varepsilon_e^{th} = 10$ MeV. Because the detection efficiency of the SK is 100 % above $\varepsilon_e \sim 8$ MeV, where ε_e is energy of electrons or positrons, we do not have to consider the detection efficiency. The energy resolution of the SK, 16 $(10\mathrm{MeV}/\varepsilon_e)^{1/2}$ (%) (Nakamura et al. 1994), is taken into account in our MC

codes assuming the Gaussian distribution. [For details of the MC data generation of water Čerenkov detectors, see, e.g., Krauss et al. (1992). Our MC simulation is basically similar to that of Krauss et al.]

The time-integrated, expected event distribution in positron or electron energy at the SK is shown in Fig. 5 for each reaction mode, for the case of a supernova at the Galactic center, i.e., $D = 10$ kpc. An example of the MC simulation is also shown as a histogram, which includes all reaction modes. Because we set $\varepsilon_e^{th} = 10$ MeV, the contamination of scattering events and oxygen events to $\bar{\nu}_e$p events is negligible. Figure 6 shows the time histogram of events of this sample data set. The numerical supernova model used here produces about 8300 events in the range of $0 \leq t \leq 18$ [sec], when $D = 10$ kpc. Most of these events are due to the $\bar{\nu}_e p$ reaction. The neutrino-electron scattering reactions produce about 200 events, and the ν_e and $\bar{\nu}_e$ absorptions into ^{16}O produce about 100. Since we cannot know the exact time of the onset of the collapse, we set the time of the first event to zero.

The neutronization burst, namely, a strong peak in ν_e luminosity (reaching $\sim 5 \times 10^{53}$ erg/sec after 3–4 msec after the core bounce) when the shock wave passes the neutrino sphere has attracted great attention of researchers because its signal could be used for probing the electron neutrino mass or probing the neutrino oscillation such as $\nu_e \leftrightarrow \nu_\mu$ or ν_τ. It is also expected that this signal is more energetic if the delayed explosion mechanism obtains rather than the prompt mechanism (Burrows et al. 1992). However, the burst duration is $\sim$ a few msec and emitted energy as ν_e's is therefore only several $\times 10^{51}$ erg. In addition, the cross section of $\nu_e e$ scattering is about 1–2 orders of magnitude lower than that of the $\bar{\nu}_e p$ reaction, and hence it is doubtful that we can clearly recognize the neutronization burst even in the case of a Galactic supernova detected by the SK. During the neutronization burst, the average energy of ν_e's is ~ 11 MeV and expected number of scattering events is $\sim 2.7(E_{\nu_e}/10^{51}\text{erg})$. Figure 7 shows an example of the MC simulation for very early events including the neutronization burst; the solid line is for electron scattering events mainly due to ν_e's, while the dashed line is for $\bar{\nu}_e p$ events. Although the scattering events are strongly forward peaked, it seems difficult to distinguish the neutronization burst from $\bar{\nu}_e p$ events when we take account of the angular resolution of the SK ($\sim 30^\circ$).

4. Statistical Analysis for Reconstruction of $\bar{\nu}_e$' Flux and Spectrum

4.1. Time-binning: the Simplest Analysis

In the following part of this paper we consider reconstruction of $\bar{\nu}_e$ flux and spectrum from $\bar{\nu}_e p$ events. In order to seek the signature of the delayed explosion mechanism, we have to reconstruct the time evolution of $\bar{\nu}_e$ luminosity and spectrum during the first 1 sec after the bounce. The simplest procedure to do this is to divide the time coordinate into many bins and estimate the luminosity and average energy in each time-bin. Let N_i, $(\Delta t)_i$, and $(\bar{\varepsilon}_e)_i$ be number of events, width, and average energy of positrons or electrons in the i-th bin, in the energy range where analysis is performed. As mentioned in §3, we take this energy range as $\varepsilon_e > \varepsilon_e^{th}$= 10 MeV. In the following analysis, we assume the Fermi-Dirac distribution with a single temperature and zero chemical potential for the simplicity. As discussed in Introduction, this assumption is clearly oversimplification, but since we are interested in the time evolution of $\bar{\nu}_e$ luminosity and average energy, this assumption does not affect the conclusion seriously. Note that the analyzed MC data are generated by a numerical simulation of multi-energy-group neutrino diffusion which does not assume any shape of neutrino spectrum. This makes it possible for us to investigate whether we can see the deviation of the neutrino spectrum from the pure FD distribution by comparing the FD fits to energy distributions of MC data. We have also tried a fit with time-evolving, nonzero chemical potential in FD distribution, but it is found that we cannnot constrain strongly the chemical potential, if we set a rather high threshold, ε_e^{th}= 10 MeV.

We can then easily estimate the luminosity $L^i_{\bar{\nu}_e}$ and effective temperature $T^i_{\bar{\nu}_e}$ in the i-th bin by solving the following equations:

$$(\Delta t)_i \int_{\varepsilon_e^{th}}^{\infty} d\varepsilon_e \, \frac{d^2N(\varepsilon_e; L^i_{\bar{\nu}_e}, T^i_{\bar{\nu}_e})}{dt d\varepsilon_e} = N_i \ , \tag{6}$$

$$\int_{\varepsilon_e^{th}}^{\infty} d\varepsilon_e \, \varepsilon_e \frac{d^2N(\varepsilon_e; L^i_{\bar{\nu}_e}, T^i_{\bar{\nu}_e})}{dt d\varepsilon_e} = (\bar{\varepsilon}_e)_i \int_{\varepsilon_e^{th}}^{\infty} d\varepsilon_e \, \frac{d^2N(\varepsilon_e; L^i_{\bar{\nu}_e}, T^i_{\bar{\nu}_e})}{dt d\varepsilon_e} \ , \tag{7}$$

where $d^2N/dtd\varepsilon_e$ is the expected event rate per unit time per unit energy, which is generally given in the following form:

$$\frac{d^2N}{dtd\varepsilon_e} = \sum_l \sum_m \int_0^{\infty} d\varepsilon_\nu \, \frac{dF^l(\varepsilon_\nu)}{d\varepsilon_\nu} \, \frac{d\sigma^{lm}(\varepsilon_\nu, \varepsilon_e)}{d\varepsilon_e} \, N^m_{\rm target} \, \epsilon(\varepsilon_e) \ . \tag{8}$$

In the above expression, l and m run all neutrino types and possible reactions, respectively, and ε_ν is neutrino energy, $dF/d\varepsilon_\nu$ differential number flux of neutrinos per unit neutrino energy, $d\sigma/d\varepsilon_e$ differential cross section, $N_{\rm target}$ total number of target particles in the detector, and $\epsilon(\varepsilon_e)$ the detection efficiency (100 % if $\varepsilon_e > \varepsilon_e^{th}$). Although the sample data set generated from the MC code includes all reactions in Eq. (1)–(5), we analyze the

data considering only the dominant $\bar{\nu}_e p$ reaction for simplicity. In this approximation, the differential cross section is (Vogel 1984; Burrows 1988)

$$\frac{d\sigma_{\bar{\nu}_e p}}{d\varepsilon_e} = \frac{1}{4}\sigma_0(1+3\alpha^2)(1+\delta_{\rm WM})\ \frac{\varepsilon_e p_e c}{(m_e c^2)^2}\ \delta(\varepsilon_\nu - \varepsilon_e - \Delta_{np})\ , \tag{9}$$

where $\sigma_0 = (2G_F m_e \hbar)^2/\pi c^2$, α the axial-vector coupling constant (~ -1.26), p_e positron momentum, and Δ_{np} the neutron-proton mass difference (1.294 MeV). The weak-magnetism correction, $\delta_{\rm WM}$, is approximately $-0.00325\ (\varepsilon_\nu - \Delta_{np}/2)/{\rm MeV}$. The $\bar{\nu}_e$ number flux, $dF_{\bar{\nu}_e}/d\varepsilon_\nu$, is expressed as

$$\frac{dF_{\bar{\nu}_e}}{d\varepsilon_\nu} = \frac{L_{\bar{\nu}_e}}{4\pi D^2 T_{\bar{\nu}_e}^4 F_3(\eta)}\ \frac{\varepsilon_\nu^2}{e^{\beta(\varepsilon_\nu-\mu)}+1}\ , \tag{10}$$

where μ is the chemical potential, $\beta = T_{\bar{\nu}_e}^{-1}$, $\eta = \mu/T_{\bar{\nu}_e}$, (the Boltzman constant is set to the unity) and $F_n(\eta)$ is defined as

$$F_n(\eta) \equiv \int_0^\infty \frac{x^n}{e^{x-\eta}+1} dx\ . \tag{11}$$

In the following analysis we set $\eta = 0$ and assume that the distance to the supernova is known. If the distance is uncertain in practical analysis in the future, the luminosity should be replaced by the bolometric flux, i.e., $F_{\bar{\nu}_e} = L_{\bar{\nu}_e}/4\pi D^2$.

We show a result of this time-binning analysis on a sample data set ($D = 10$ kpc) in Fig. 8. Luminosity and average energy of $\bar{\nu}_e$'s above $\varepsilon_\nu > (\varepsilon_e^{th} + \Delta_{np})$, which are calculated from $L^i_{\bar{\nu}_e}$ and $T^i_{\bar{\nu}_e}$ obtained by solving the Eqs. (6) and (7), are shown as the data points. The time bins are defined so that the event numbers in each bin are the same among the bins. The number of events in one bin is ~ 400 in this figure. The statistical errors can approximately be estimated as

$$\mathrm{Err}(L_{\bar{\nu}_e}) = \frac{1}{\sqrt{N_i}} \qquad (\%)\ , \tag{12}$$

$$\mathrm{Err}(T_{\bar{\nu}_e}) = \frac{1}{\sqrt{N_i}}\ \frac{(\sigma_\varepsilon)_i}{(\bar{\varepsilon}_e)_i} \qquad (\%)\ , \tag{13}$$

where $(\sigma_\varepsilon)_i$ is the observed standard deviation of ε_e in the i-th bin. The error in luminosity is inferred from Poissonian statistics and that in temperature from the statistical 1 σ error in the observed $(\bar{\varepsilon}_e)_i$. Dashed lines are luminosity and average energy of the numerical supernova model above $\varepsilon_\nu = (\varepsilon_e^{th} + \Delta_{np})$. It should be noted that we cannot know the offset time of the first event in a future detection, but for the purpose of comparison, we plot the fitted results in the same time coordinate with the numerical supernova model unless otherwise stated. The obtained luminosity and average energy well agree with those

of the original numerical supernova model. Although the fitted average energy seems systematically lower than the original because of the deviation from the FD distribution or contamination of reactions other than $\bar{\nu}_e p$, this systematic error is sufficiently small. However, it should be noted that significant systematic errors emerge when we extrapolate the obtained neutrino spectrum down to lower energy range below the threshold with the assumed FD distributions. Figure 9 is the same as Figure 8, but for the whole energy range including $\varepsilon_\nu < (\varepsilon_e + \Delta_{np})$. It is clear that an analysis assuming the FD distribution leads to systematic overestimation in luminosity and underestimation in average energy, because the spectrum with obtained $T^i_{\bar{\nu}_e}$ significantly overestimates the neutrino flux below the threshold energy. This comes from the fact that spectrum of numerical supernova models is 'pinched', i.e., deficient in both low- and high-energy range compared to the pure FD distribution.

The features of the delayed mechanism discussed in §2 can be seen clearly by this simple analysis. Therefore a supernova at the Galactic center is near enough to get information for the explosion mechanism. Now let us consider a case when a supernova is more distant from the Earth. Figure 10 is the same as Figure 8, but for a supernova at the LMC ($D = 50$ kpc). The event number in each time bin is about 30. The statistical errors become larger and the features of the explosion mechanism are obscured by the bin width and statistical errors. It is difficult to reconstruct a smooth time evolution from these discrete data points. Here we point out that although the time-binning analysis is simple and easy, this method loses some important information and we can reproduce a smooth evolution more efficiently by other methods of analysis. In the next section, we discuss the information loss in the time-binning analysis and propose a new method which uses a likelihood function and cubic-interpolation.

4.2. Likelihood Analysis with Cubic-Spline Interpolation

The time-binning analysis is simple and clear, but it loses some important information in the following two points. First, the detection time of each event is smoothed out in the time bin in which the event is included. Generally water Čerenkov detectors have fairly good time resolution (much better than msec), but the time-binning analysis cannot extract any information on the time scale shorter than the bin width. Second, the events in a bin are treated independently of those in other bins, and this leads to statistical fluctuation in the obtained results between neighboring bins. If we assume the time evolution is smooth, we can suppress the statistical fluctuation to some extent by smoothing. We consider here an analysis method which is more effective in the above two points than the time-binning

analysis.

In order not to lose any information about detection time of each event, we use the well-known maximum likelihood analysis, where the likelihood function for the analysis of supernova neutrinos is given as

$$\mathcal{L} \equiv \log L = \sum_{j=1}^{N_{obs}} \ln \left(\frac{d^2N(t^j, \varepsilon_e^j)}{dtd\varepsilon_e} \right) - \int_{t_l}^{t_u} dt \int_{(\varepsilon_e)_l}^{(\varepsilon_e)_u} d\varepsilon_e \frac{d^2N}{dtd\varepsilon_e} \ , \tag{14}$$

where t^j and ε_e^j are detection time and energy of j-th event, $N_{\rm obs}$ the total number of events, and t_l, t_u, $(\varepsilon_e)_l$, and $(\varepsilon_e)_u$ are the boundaries of the analysis region in the $(t,\ \varepsilon_e)$ space, which can be set arbitrarily. [For the derivation of this function, see, e.g., Loredo & Lamb (1989).] Because we are interested in the time evolution, we assume the FD distribution with $\eta = 0$ for energy spectrum. Then expected $d^2N(t, \varepsilon_e)/dtd\varepsilon_e$ can be calculated if the time evolution of $L_{\bar{\nu}_e}$ and $T_{\bar{\nu}_e}$ is given. Generally this time evolution is modeled by some analytic functions, e.g., exponential or power-law decay, but the time evolution with which we are concerned cannot be modeled with any simple functions. We therefore set some grid points in the time coordinate, t_k, $(k = 1, \ldots, N_{\rm grid})$ and L_k and T_k are defined as $L_{\bar{\nu}_e}(t_k)$ and $T_{\bar{\nu}_e}(t_k)$, respectively. We model $L_{\bar{\nu}_e}(t)$ and $T_{\bar{\nu}_e}(t)$ by the natural-cubic-spline interpolation in order to reproduce a smooth evolution. The merit of use of this interpolation is not only that we can get a smooth time evolution, but the statistical fluctuation is also suppressed. The reason is as follows. Most methods for smooth interpolation, including the natural-cubic-spline, are generally unstable to random fluctuation between the neighboring grids, or to a random pattern. If the values of L_k and T_k become unrealistically random, values of $L_{\bar{\nu}_e}$ and $T_{\bar{\nu}_e}$ at points between the defined grids will become artificially oscillatory and then the likelihood function evaluated with cubic-spline interpolation will become lower. Therefore this method is expected to suppress unnecessary statistical fluctuation in time evolution.

Now we can find the best-fit time evolution in $L_{\bar{\nu}_e}$ and $T_{\bar{\nu}_e}$ by searching maximum of $\mathcal{L}$ in the model parameter space, $\{L_k, T_k\}$. We have adopted this analysis method to the MC data for a supernova at $D = 10$ and 50 kpc, and the results about the luminosity and average energy above the threshold energy $(\varepsilon_e^{th} + \Delta_{np})$ are shown in Figs. 11 and 12. We set the time grids so that the event numbers per one time grid is ~ 800 and ~ 60 for $D = 10$ and 50 kpc, respectively, and these grids are expressed as crosses in the figures. The best-fit curves of both cases (solid lines) well reproduce the smooth time evolution of the original numerical supernova model (dashed lines). These results should be compared with those of the time-binning analysis shown in Figs. 8 and 10, and it can be seen that this method is useful to reconstruct a smooth and natural time evolution especially when a supernova is distant and available events are fewer. For the $D = 10$ kpc case the difference of the

two methods is not so important because of rich statistics, but the initial steep rise of the luminosity curve can better be reproduced by the likelihood analysis than the time-binning analysis. In order to show the statistical uncertainties in the above analysis, we make other five data sets of MC simulation from the same numerical supernova model for the $D = 50$ kpc case, and do the same analysis for all of them. The results are shown in Fig. 13, and this figure should be compared to the statistical errors in Fig. 10.

The number of grid points defined on the time coordinate is crucially important in the above analysis. We should choose a sufficient number of grids which can resolve the time scale in which we are interested, but it is apparent that if we set too many time grids, the statistical fluctuation per one grid will become larger and obtained results become unstable. In Figs. 14 and 15, we show the result of the same analysis about the $D = 50$ kpc data with different number of grids; the number of grid points is increased by factors of 2 and 4 from that in Fig. 12, respectively. The instability can be seen clearly, and therefore discrimination of the true time evolution from sham evolution due to statistical fluctuation is important. In a practical analysis in the future, we should try various intervals of grids taking account the statistical errors estimated by the time-binning analysis. The goodness-of-fit test, which we discuss in the next section, will also help us to discriminate a true evolution from statistical fluctuations. If we get sufficient goodness-of-fit with a given number of grids, the analysis with more grids is unnecessary.

4.3. Goodness-of-Fit test and Deviation from the FD distribution

Generally a statistical analysis includes the following three procedures: 1) find the best fit parameters, 2) estimate the statistical errors, and 3) check whether the best-fit model is consistent with the observed data. Here we consider the third procedure, a so-called goodness-of-fit (GOF) test. If a likelihood function is given with some assumptions about the model, it is rather a straightforward process to find the best-fit parameters. However, the likelihood analysis itself does not verify the assumed model, and therefore we have to check whether the observed data naturally come out from the assumed model with best-fit parameters. We use the two-dimensional version of the Kolmogorov-Smirnov (KS) test (Peacock 1983; Fasano & Fianceschini 1987) as a tool of the GOF test. The KS measure $D_{\rm KS}$, which is a measure of deviation of the observed data from the best-fit model, is defined as follows. First, we define the expected and observed fraction of events in the four quadrants of (t, ε_e) space:

$$f^l_{\rm exp}(t, \varepsilon_e) = \frac{1}{N_{\rm exp}} \iint_l dt' d\varepsilon'_e \frac{d^2N(t', \varepsilon'_e)}{dt d\varepsilon_e} \ , \tag{15}$$

and $f^l_{\rm obs}(t,\varepsilon_e) = N^l_{\rm obs}(t,\varepsilon_e)/N_{\rm obs}$, where l (= 1, 2, 3, and 4) denotes the four quadrants: $(t' < t, \varepsilon'_e < \varepsilon_e)$, $(t' > t, \varepsilon'_e < \varepsilon_e)$, $(t' < t, \varepsilon'_e > \varepsilon_e)$, and $(t' > t, \varepsilon'_e > \varepsilon_e)$. The quantity $N^l_{\rm obs}(t,\varepsilon_e)$ is the number of events in the l-th quadrant, and $N_{\rm exp}$ is the total expected number of events in the whole analysis region. Then D_{KS} is defined as the maximum of the absolute difference of $f^l_{\rm exp}$ and $f^l_{\rm obs}$, i.e.,

$$D_{KS} = \max_{l,\ t,\ \varepsilon_e} |f^l_{\rm exp}(t,\varepsilon_e) - f^l_{\rm obs}(t,\varepsilon_e)| \ . \tag{16}$$

We can check the consistency between the observed data and the best-fit model by comparing D_{KS} of the observed data and probability distribution of D_{KS} expected from the best-fit model. The probability distribution of D_{KS} is unknown in this two dimensional case, and we have to estimate this by a number of MC simulations.

We have applied this test on the results obtained by the likelihood analysis in the previous section for both the D = 10 and 50 kpc cases (Fig. 11 and 12), by using the probability distribution of D_{KS} obtained by 100 MC simulations. It is found that the best-fit model and the MC data are statistically consistent for the D = 50 kpc case, but inconsistent for the D = 10 kpc case with more than 99 % C.L. Because the time evolution is considered to be modeled appropriately, this suggests that the inconsistency comes from the assumption of the FD distribution in energy spectrum. This means that, in other words, we can distinguish the difference of the real spectral shape of supernova $\bar{\nu}_e$'s from pure FD distributions when a supernova occurs nearer than 10 kpc. In order to demonstrate this, we plot the time-integrated energy spectrum of events expected from the best-fit model obtained by the likelihood analysis assuming the FD distribution, by the dashed line in Fig. 16 for the D = 10 kpc case. The histogram is the analyzed MC data and the solid line is the expected spectrum of the numerical model from which the MC data are generated. The difference of the dashed line from the histogram is clearly discernible; overestimation at $\varepsilon_e < 18$ MeV and underestimation at $\varepsilon_e > 18$ MeV. This deviation should be considered as a prediction of a standard picture of neutrino emission from collapse-driven supernovae and can be tested in a future observation. Figure 17 is the same as Figure 16, but for the D = 50 kpc case. In this case it seems difficult to see the deviation from the FD distribution, and this is consistent with the results of the GOF test.

5. Discussion

Neutrino-driven Rayleigh-Taylor instabilities between the stalled shock wave and the neutrinospheres are generic feature of collapse-driven supernovae (Bethe 1990; Herant, Benz, & Colgate 1992; Herant et al. 1994; Burrows, Hayes, & Fryxell 1995; Janka &

Müller 1996; Mezzacappa et al. 1996). Such instability ineviably leads to convective motion in the energy gain region and asphericity in the dynamics, that should have significant effects on the explosion mechanism (see, e.g., Burrows 1997 for a review). Although the presented 1-D calculation takes account of convective motion by the mixing length theory, there may be some effects that can not be covered by 1-D calculation. It is interesting to consider the possible signatures of such asymmetry imprinted in neutrino emission, but unfortunately at the present stage the effect of convective motion on the emergent neutrino luminosity or spectrum is poorly known. Furthermore, rotation might tend to wash out otherwise detectable flux variations due to convective motion. In fact, the Crab pulsar rotates at approximately 200 radians/sec, and this rotation will presumably smear out other underlying observable variations.

There are some interesting hints for finite neutrino masses, such as the solar neutrino problem or the atmospheric neutrino anomaly. Neutrino oscillations due to these possible masses might significantly change the emergent spectrum of neutrinos. If the vacuum mixing angle among the three generation of neutrinos is order unity, this leads to the vacuum neutrino oscillation. Because supernova neutrinos come out through very dense matter, it is also possible that the MSW neutrino oscillation occurs such as $\nu_e \leftrightarrow \nu_\mu$ (Fuller et al. 1987). Under the direct mass hierarchy of neutrinos (i.e., $m_{\nu_e} < m_{\nu_\mu} < m_{\nu_\tau}$), the MSW matter oscillation is relevant only for neutrinos and not for antineutrinos, but it is also possible that $\bar{\nu}_e$'s, which we mainly discussed in this work, experience resonant matter oscillation with ν_μ or ν_τ, due to flavor-changing magnetic moment of Majorana neutrinos [spin-flavor precession, see e.g., Totani & Sato (1996)]. These phenomena might significantly change the neutrino spectrum, and detectability of these signature will be interesting topics in future work.

6. Summary and Conclusions

We performed a statistical analysis for the future detection of a supernova neutrino burst at $D = 10$ kpc (the Galactic center) and $D = 50$ kpc (LMC) by the Super-Kamiokande detector, by using a numerical supernova model and realistic Monte-Carlo (MC) simulations of detection. We mainly discussed the detectability of the signatures of the delayed explosion mechanism in the time evolution of the $\bar{\nu}_e$ luminosity and spectrum: a hump during the first $\lesssim$ 0.5 second and following abrupt drop in the $\bar{\nu}_e$ luminosity curve, and also corresponding spectral hardening. [It should be noted that these signatures generally depend on the mass and internal structure of the progenitor star. The model used is for SN1987A, i.e., its progenitor is a $\sim 20\ M_\odot$ main-sequence star.] The ν_e neutronization burst

is considered to be more energetic for the delayed explosion and hence could be another clue to the explosion mechanism. However our simulation of the delayed explosion produces only about 5 scattering events due to neutronization burst when $D = 10$ kpc, and it seems difficult to distinguish clearly the burst from $\bar{\nu}_e p$ events.

We analyzed MC data generated from the numerical supernova model in the energy range above 10 MeV (to avoid background noise), and found the following results. 1) The signatures of the delayed explosion in $\bar{\nu}_e$ luminosity curve and spectral evolution are clearly discernible for the $D = 10$ kpc case, and moreover, the difference of the real energy spectrum from pure Fermi-Dirac (FD) distribution can also be observable. 2) For the $D = 50$ kpc case, the signature of the delayed explosion is still observable, but statistical fluctuation is too large to distinguish the deviation from the FD distribution. These results suggest that we will be able to distinguish the two proposed explosion mechanisms if a supernova occurs in Our Galaxy or Magellanic Cloulds in the near future. The deviation from the FD distribution would, if observed, provide an important test for the standard picture of neutrino emission from collapse-driven supernovae. The FD fitting leads to significant overestimation of flux in lower energy region ($\lesssim$ 15 MeV), and this results in overestimation in luminosity and underestimation in average energy. We should be careful for this in a future analysis when the obtained results are extrapolated down to the lower energy region below the threshold.

Time-binning analysis is the simplest method to reconstruct the time evolution of $\bar{\nu}_e$ flux and spectrum, but this method loses some important information and hence is not maximally effective. Therefore we proposed a method for reconstruction of the time evolution, which gives a smoother time evolution and smaller statistical errors than the simple time-binning analysis. This method is based on the likelihood analysis, and its characteristic is the use of cubic-spline interpolation to express the time evolution of $\bar{\nu}_e$ luminosity and effective temperature with some selected grid points on the time coordinate. The likelihood analysis does not lose any detection time information and the stability of the cubic-spline interpolation to random fluctuation suppresses statistical fluctuations. This method is useful especially when available number of events is relatively small, e.g., a supernova in the LMC or SMC.

This work has been supported in part by the Grant-in-Aid (KS) for the Center-of-Excellence Research No. 07CE2002 and (TT) for the Scientific Research Fund No. 3730 of the Ministry of Education, Science, and Culture in Japan. This work was also supported by (HED and JRW) DOE Contract No. W-7405-ENG-48 and (JRW) NSF Grant No. PHY-9401636.

REFERENCES

Arnett, W. D. 1983, ApJ, 263, L55

Baron, E., Cooperstein, J., & Kahana, S. 1985, Phys. Rev. Lett., 55, 126

Bethe, H. A. & Wilson, J. R. 1985, ApJ, 295, 14

Bethe, H. A. 1990, Rev. Mod. Phys. 62, 801

Bionta R. M. et al. 1987, Phys. Rev. Lett., 58, 1494

Bratton C. B. et al. 1988, Phys. Rev. D, 37, 3361

Bruenn, S. 1987, Phys. Rev. Lett., 59, 938

Burrows, A. 1988, ApJ, 334, 891

Burrows, A., Klein, D., & Gandhi, R. 1992, Phys. Rev. D, 45, 3361

Burrows, A., Hayes, J. & Fryxell, B. A. 1995, ApJ, 450, 830

Burrows, A. 1997, astro-ph/9706137

Fasano, G., & Fianceschini, A. 1987, MNRAS, 225, 155

Fuller, G. M., Mayle, R. W., Wilson, J. R., & Schramm, D. N. 1987, ApJ, 322, 795

Giovanoni, P. M., Ellison, D. C., & Bruenn, S. W. 1989, ApJ, 342, 416

Haxton, W. 1987, Phys. Rev. D, 36, 2283

Herant, M., Benz, W., & Colgate, S. A. 1992, ApJ, 395, 642

Herant, M., Benz, W., Hix, R., Fryer, C., & Colgate, S. A. 1994, ApJ, 435, 339

Hillebrandt, W. 1982, A&A, 110, L3

Hillebrandt, W., Nomoto, K., & Wolff, R. G. 1984, A&A, 133, 175

Hirata, K. S. et al. 1987, Phys. Rev. Lett., 58, 1490

Hirata, K. S. et al. 1988, Phys. Rev. D, 38, 448

Janka, H.-T. & Hillebrandt, W. 1989, A&A, 224, 49

Janka, H.-T. & Müller, E. 1996, A&A, 306, 167

Krauss, L. M., Romanelli, P., Schramm, D., & Lehrer, R. 1992, Nucl. Phys. B, 380, 507

Langanke, K., Vogel, P., & Kolbe, E. 1996, Phys. Rev. Lett., 76, 2629

Loredo, T. J. and Lamb, D. Q. 1989, Ann. N.Y. Acad. Sci., 571, 601

Mayle, R. 1985, Ph. D. Thesis, Univ. of California

Mayle, R., Wilson, J. R., & Schramm, D. N. 1987, ApJ, 318, 288

Mezzacappa, A. et al. 1996, ApJ, in press.

Myra, E. S. & Burrows, A. 1990, ApJ, 364, 222

Nakamura, K., Kajita, T., Nakahata, M., & Suzuki, A. 1994, in Physics and Astrophysics of Neutrinos, ed. M. Fukugita and A. Suzuki, (Tokyo: Springer-Verlag) 249

Peacock, J. A. 1983, Mon. Not. Roy. Astron. Soc., 202, 615

Totani, T. & Sato, K. 1996, Phys. Rev. D, 54, 5975

Totsuka, Y. 1992, Rep. Prog. Phys., 55, 377

Vogel, P. 1984, Phys. Rev. D, 29, 1918

Wilson, J. R. 1971, ApJ, 163, 209

Wilson, J. R. 1985, in Numerical Astrophysics, ed. Centrella, J. M., LeBlanc, J. M., & Bowers, R. L. (Boston: Jones & Bartlett), 422

Wilson, J. R., Mayle, R., Woosley, S., & Weaver, T. 1986, Ann. NY Acad. Sci., 470, 267

Woosley, S. E. and Weaver, T. 1991, private communication

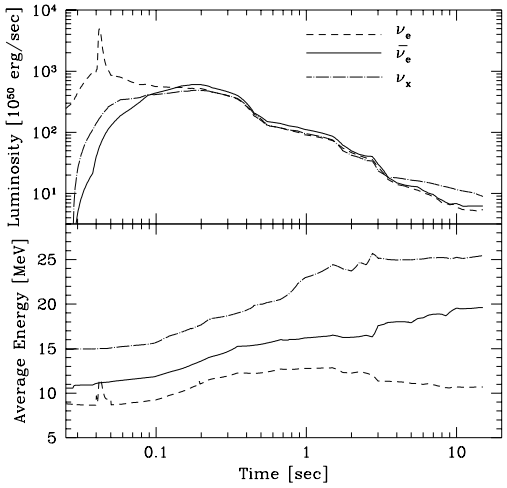

Fig. 1.— Time evolution of neutrino luminosity and average energy of the numerical supernova model used in this paper. The dashed line is for ν_e, solid line for $\bar{\nu}_e$, and dot-dashed line for ν_x (= each of $\nu_\mu, \nu_\tau, \bar{\nu}_\mu$, and $\bar{\nu}_\tau$). The core bounce time is 3–4 msec before the neutronization burst of ν_e's.

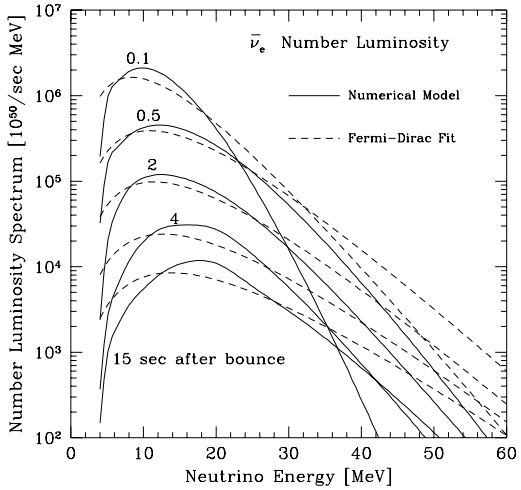

Fig. 2.— Energy spectrum of $\bar{\nu}_e$'s of the numerical supernova model used in this paper. The time (after the bounce) is indicated in the figure. The dashed lines are the Fermi-Dirac fits which have the same luminosity and average energy with the numerical model. The chemical potential is set to zero for the FD distribution.

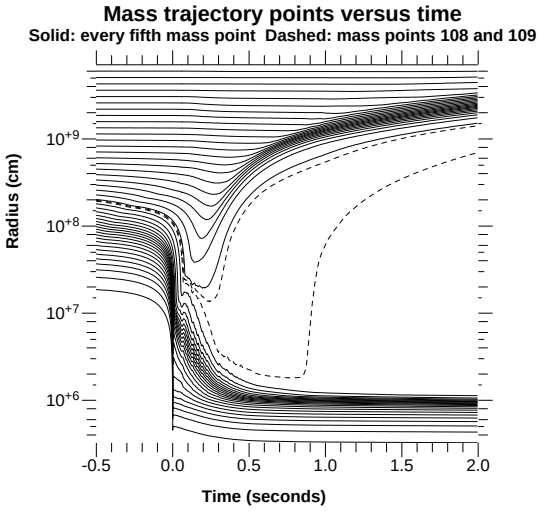

Fig. 3.— Radius as a function of time for selected mass points of the numerical supernova model used in this paper. Solid lines are drawn for every fifth mass point, while the dashed lines are for two succeeding mass points near the edge of the nascent neutron star and ejected matter.

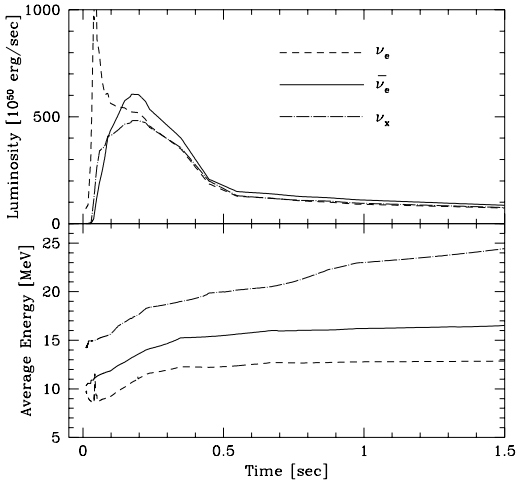

Fig. 4.— The same as Fig. 1, but for the early phase in linear coordinate.

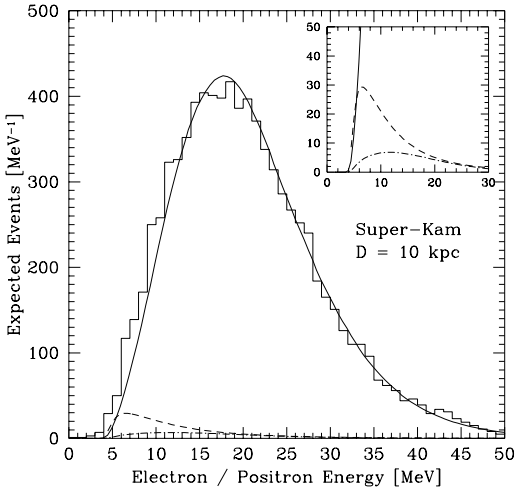

Fig. 5.— Time-integrated energy distribution of election or positron events at the Super-Kamiokande detector for a supernova at 10 kpc away from the Earth. The solid line shows the expected distribution of $\bar{\nu}_e p$ events from the numerical supernova model. The dashed and dot-dashed lines are for neutrino-electron scattering events (including all flavors of neutrinos) and $\nu_e(\bar{\nu}_e)^{16}$O events, respectively. The histogram is an example of MC simulations generated from the numerical supernova model, including all reaction modes. The inset is a magnification of the lower energy region.

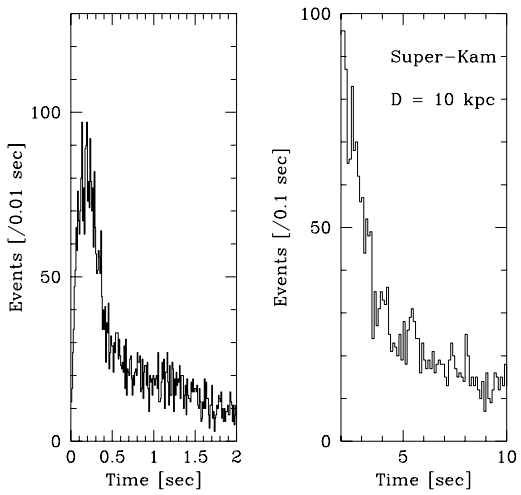

Fig. 6.— Time histogram of an example of MC simulations of the Super-Kamiokande detection generated from the numerical supernova model. The distance to the supernova is set to 10 kpc. The time of first event is set to zero.

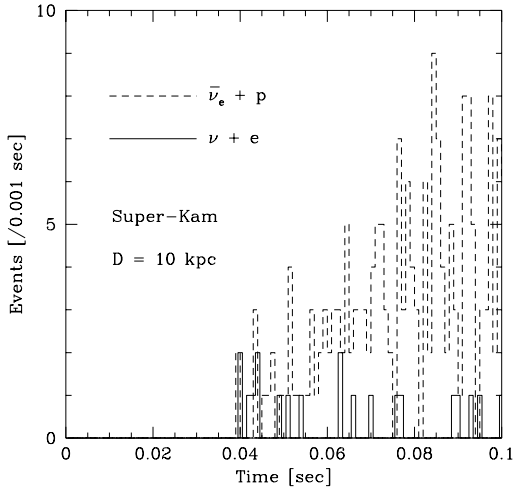

Fig. 7.— The same as Fig. 6, but for very early phase including the neutronization burst. The solid line for the neutrino-electron scattering events of all neutrino flavors, and dashed line for events of $\bar{\nu}_e p$ reactions.

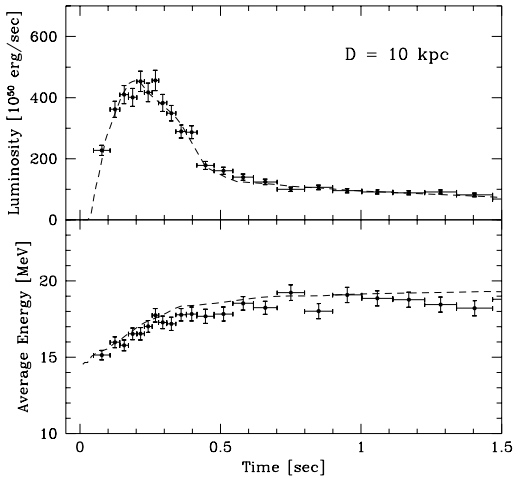

Fig. 8.— Data points are results of the time-binning analysis for a set of MC data of the SK detection of a supernova at the Galactic center ($D = 10$ kpc). The luminosity and average energy are those of $\bar{\nu}_e$'s above the threshold energy, $\varepsilon_e^{th} + \Delta_{np} = 11.3$ MeV. The vertical error bars attached on the data points indicate statistical 1 sigma errors, while the horizontal bars represent the bin width. The dashed lines are luminosity and average energy of the numerical supernova model (also above $\varepsilon_e^{th} + \Delta_{np}$) from which the MC data are generated. One time-bin includes about 400 events.

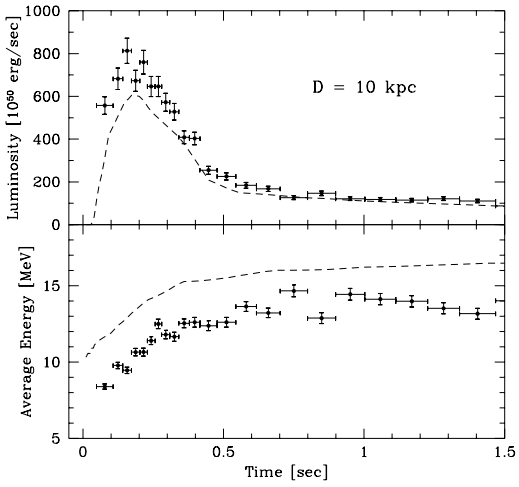

Fig. 9.— The same as Fig. 8, but for the luminosity and average energy of $\bar{\nu}_e$'s in the whole energy range including the lower energy range below $\varepsilon_e^{th} + \Delta_{np} = 11.3$ MeV.

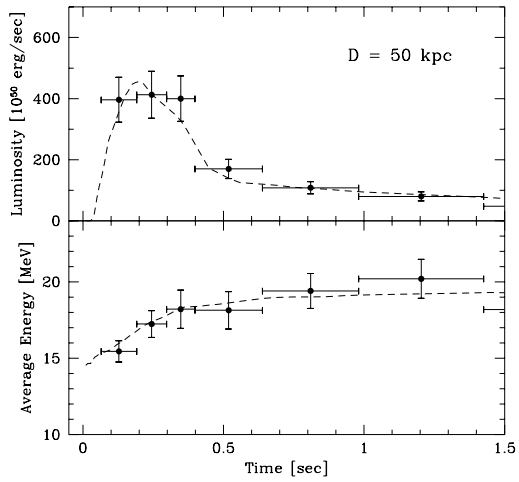

Fig. 10.— The same as Fig. 8, but for a supernova at the Large Magellanic Cloud ($D = 50$ kpc). One time-bin includes about 30 events.

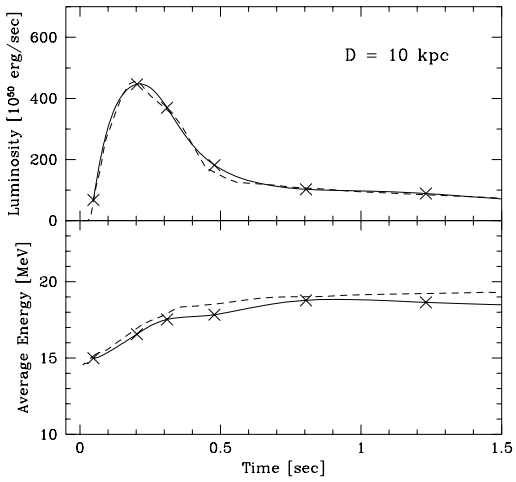

Fig. 11.— The result of the likelihood analysis for a set of MC data of the SK detection of a supernova at the Galactic center ($D = 10$ kpc). The luminosity and average energy are those of $\bar{\nu}_e$'s above the threshold energy, $\varepsilon_e^{th} + \Delta_{np} = 11.3$ MeV. The crosses are the grid points on the time coordinate, and the solid lines are the cubic-spline interpolation (see text). The dashed lines are luminosity and average energy of the numerical supernova model (also above $\varepsilon_e^{th} + \Delta_{np}$) from which the MC data are generated. The number of events per one grid point is about 800.

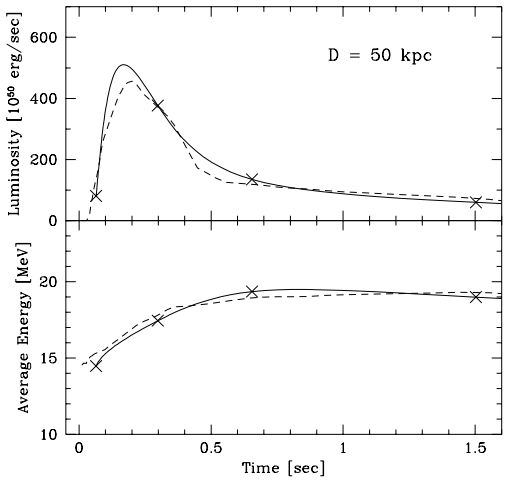

Fig. 12.— The same as Fig. 11, but for a supernova at the LMC ($D = 10$ kpc). The number of events per one grid is about 60.

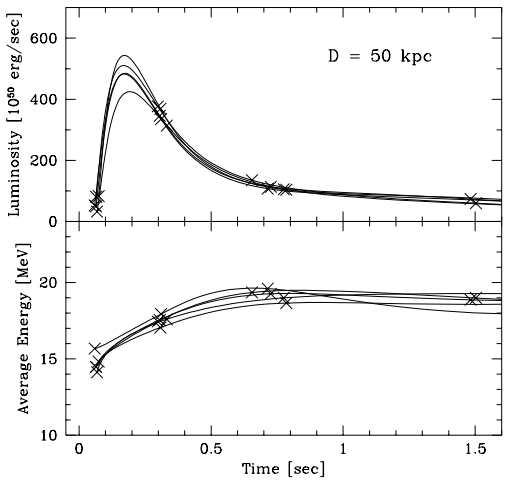

Fig. 13.— The same as Fig. 12, but for other five sets of MC data generated from the same numerical supernova model. Statistical fluctuations in the obtained results can be seen.

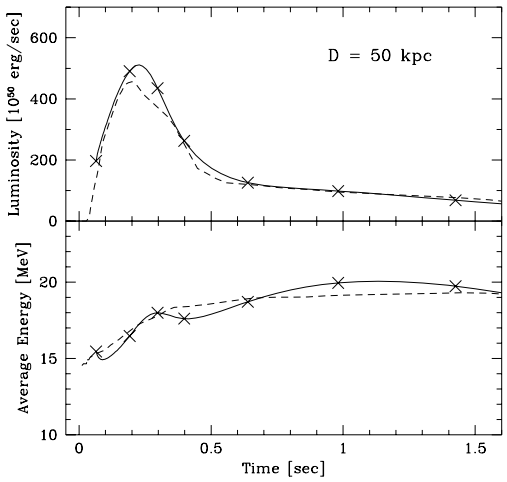

Fig. 14.— The same as Fig. 12, but the number of grid points is increased by a factor of 2.

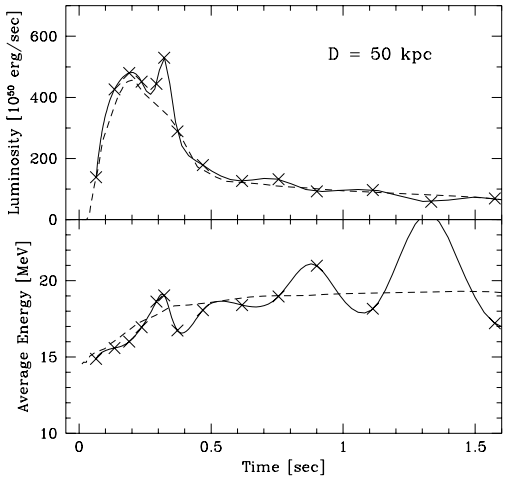

Fig. 15.— The same as Fig. 12, but the number of grid points is increased by a factor of 4.

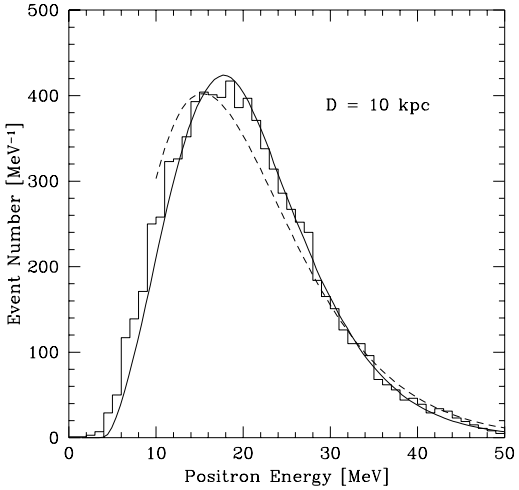

Fig. 16.— Time-integrated energy distribution of events at the SK for a supernova at the Galactic center ($D = 10$ kpc). The histogram is the MC data analyzed, and the solid line is the distribution of $\bar{\nu}_e p$ events expected from the numerical supernova model from which the MC data are generated. The dashed line is the best-fit distribution determined by the likelihood analysis (Fig. 11) assuming the Fermi-Dirac (FD) distribution ($\mu = 0$). The difference of the FD fit and the MC data is clear.

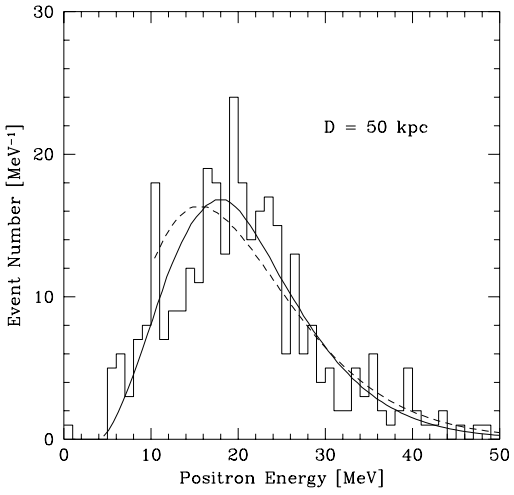

Fig. 17.— The same as Fig. 16, but for a supernova at the LMC ($D = 50$ kpc). The deviation of the FD fit from the MC data cannot be distinguished from statistical fluctuations.